FUDMA Journal of Sciences (FJS)
ISSN online: 2616-1370
ISSN print: 2645 - 2944
Vol. 9 No. 1, January, 2025, pp 63 - 73
DOI: https://doi.org/10.33003/fjs-2025-0901-2810

EXPLORING GEOTHERMAL ZONES IN NORTHERN NIGERIA USING LAND SURFACE TEMPERATURE DATA FROM REMOTE SENSING

***Joseph Aza Ahile, Osita Chukwudi Meludu and Adetola Sunday Oniku**

Department of Physics, Faculty of Physical Sciences, Modibbo Adama University, Yola, Adamawa State, Nigeria.

*Corresponding authors' email: ahilejoseph@gmail.com Phone: +2348101500437; +2347053594911

ABSTRACT

Nigeria is still unable to meet even the most basic of its energy needs, this lack of power is most evident in houses located in the North-Central and North-East areas. This paper focused on evaluating geothermal potential through remote sensing techniques in parts of Northern Nigeria. Four digital elevation model (DEM) scenes, three Landsat-9(OLI-2/TIR-2) with minimum zero or minimum cloud cover (<6%), and Terra Moderate Resolution Imaging Spectroradiometer satellite images for the research region were processed using ArcMap 10.7.1, Google Earth Pro, and QGIS 3.36.3. The linear correlation analysis performed between Landsat LST and MODIS LST images showed a high correlation coefficient ($R^2 = 0.907$). Anomalously high lineament density correlates with high land surface temperature, dominantly in the basement complex of the study area; it's possible that the fracturing will increase the permeability, enabling warm or hot springs to rise to the surface. Fault lines that permit the movement of hot/warm water to the Earth's surface can be linked to active geothermal zones. The stream/rivers in or around the targeted high LST are probably thermal springs, as they were overlaid on the LST, and high-temperature spots($>28^0$) were identified. The regions around Jibam, Langtang, Aikri, Adikpo, Shemdam, and Ashinge prove to be areas where warm or hot springs can be located.

Keywords: Land Surface Temperature, LandSat-9(OLI-2/TIR-2), MODIS_LST, Lineament density, Warm/hot spring

INTRODUCTION

Given the global population expansion, rising living standards, and swift industrialization, future energy consumption is anticipated to be enormous. The deficient energy supply hampers socioeconomic activity, limits economic progress, and adversely impacts quality of life (Oseni, 2011). Energy cannot be replaced in critical sectors of the economy, including industry, agriculture, transportation, and services. Considering the critical role that energy plays in a country's ability to grow economically, prosper, and develop as well as in eradicating poverty and ensuring national security, Nigeria is still unable to meet even the most basic of its energy needs. In contrast, most developed nations are competing for renewable energy due to global warming and the necessity to transition to a human society with little impact on the environment (Newell & Bulkeley, 2017). This absence of electricity in Nigeria is most visible among households in the North-East and North-Central regions (Sasu,2023).

In 2023, more than 60% of the electricity produced worldwide came from fossil fuels, even with renewable energy sources being aggressively rolled out in all major economies (Littleton, Colorado, Nov. 30 (Reuters)). Ember, a think tank, predicts that several important countries, like; the US (59%), China (65%), India (75%), Japan (63%), Poland (73%), and Turkey (57%), sourced far over half of their power from petroleum and natural gas in 2023. Since 2019, the quantity of power generated globally from renewable energy sources has risen at a rate that is more than three times faster than that of fossil fuels, which has given advocates of the energy shift from coal, oil, and natural gas impetus. However, according to Ember statistics, the percentage of clean electricity generated globally was still below 40% during the January to August period of 2023, suggesting that fossil fuels will continue to be the world's leading source of electricity (Maguire, 2023).

In Nigeria, coal, oil, gas, and water are the main energy sources used to produce power. Fossil fuels provided 22 terawatt hours of electricity in 2020. That year, natural gas sources accounted for the largest share of fossil fuel power generation (Sasu, 2022). Because fossil fuel use results in environmental damage, there is a major energy concern. The region has to look into alternate renewable energy sources because fossil fuels are finite, unreliable, and have negative environmental effects. Nigeria has a wealth of renewable energy resources that, if used efficiently to generate electricity, might improve its supply, particularly in rural areas (Newsom, 2012). The quest for alternative renewable energy sources, such as geothermal energy, has been prompted by the depletion of fossil fuels, their unpredictability, and their effects on the environment. When used appropriately and efficiently, these resources will offer a reliable, sustainable, and alternative energy source that will help solve the issue of an intermittent energy supply and reduce the over-reliance on petroleum and petroleum-derived products, which negatively impacts the ecosystem (Ahile *et al*,2024). According to Abraham *et al*. (2015), geothermal energy may represent a significant long-term goal for clean energy sources. Given its established reliability, cleanliness, and safety, geothermal energy is considered to be one of the most attractive sources of environmentally friendly energy; as a result, its use in power generation, heating, and cooling is growing (Kömürcü & Akpınar, 2009).

Recent developments in the deployment of airborne technologies for remote sensing have shown the potential of remotely sensed Thermal Infrared (TIR) imagery for geothermal investigation. The temperature anomalies linked to surface geothermal structures including fumaroles, hot springs, geysers, and warmed ground could be identified and measured using TIR remote sensing data. When using TIR remote sensing to look for surface temperature variations that might be connected to geothermal resources, land surface temperature (LST) is an essential parameter (Sekertekin and Arslan, 2019). According to Rajeshwari and Mani (2014), Land Surface temperature (LST) is the temperature felt on the ground when one's hands are placed there or the earth's surface temperature. Land Surface Temperature (LST)

assessment is achievable with the incorporation of thermal band (TIR 10 and 11) in Landsat-8 and Landsat-9 images. The satellite sensors systematically gather high-quality images of the planet's surface. The number of built surfaces, the agricultural-related studies, the health and type of vegetation, geothermal research, and many more applications are all determined by satellite data. This is due to its simplicity of use, rapidity, precision, affordability, and coverage. Recent developments in digital and satellite technology have also resulted in a notable improvement in this technique (Onyewuchi *et al*., 2012). In contrast to prior satellites that only had a single sensor, Landsat 9 gathers information from two different sensors namely: an Operational Land Imager (OLI-2) and a Thermal Infrared Sensor (TIRS-2) in 11 bands. Improvements made to Landsat 9 include improved radiometric resolution for OLI-2 (14-bit quantization compared to 12-bits for Landsat 8), which enables sensors to automatically pick up on more minute variations, particularly over darker regions like dense forests or water. The OLI-2 upgrade, in conjunction with TIRS-2, has significantly reduced stray light relative to the Landsat 8 Thermal Infrared Sensor (TIRS), facilitating improved atmospheric correction and more accurate surface temperature measurements. The two spectral bands that TIRS-2 offers have a maximum ground sampling distance of 100 m (328 ft) for both in-track and cross-track. In addition to space view capabilities, TIRS-2 has an inbuilt blackbody calibration source (Shahfahad et al, 2022; Eon et al, 2024). The instruments on Landsat 9 were designed as improved copies of the Landsat 8 sensors as shown in Table 1

Table 1: Band characteristics of the Landsat-9 operational land imager (OLI-2) and Thermal infrared (TIR-2) sensors (Source: USGS)

Band	Name	Wavelength(μm)	Spatial Resolution(m)	Useful for mapping
1	Visible costal Aerosol	0.43-0.51	30	Coastal and aerosol studies
2	Visible Blue	0.45-0.51	30	Bathymetric mapping, distinguishing soil from vegetation and deciduous from coniferous vegetation
3	Visible Green	0.53-0.59	30	Emphasizes peak vegetation, which is useful for assessing plant vigor
4	Red	0.64-0.67	30	Discriminates vegetation slopes
5	Near-infrared	0.85-0.88	30	Emphasizes biomass content and shorelines
6	SWIR 1	1.57-1.65	30	Discriminates moisture content of soil and vegetation; penetrates thin clouds
7	SWIR1 2	2.11-2.29	30	Improve moisture content of soil and vegetation; penetrate thin clouds
8	Panchromatic	0.50-0.68	15	Sharper image definition
9	Cirrus	1.36-1.38	30	Improved detection of cirrus cloud contamination
10	TIRS 1	10.60-11.19	100	Thermal mapping and estimated soil moisture
11	TIRS 2	11.50-12.51	100	Improved thermal mapping and estimated soil moisture

Table 2: Characteristics of MOD11A1 V006 MODIS /Tera Land Surface Temperature/Emissivity (Dervisoglu, 2013)

Earth Science Data Type	Spectral Resolution (μm)	Spatial Resolution	Temporal Resolution	Number Type
MOD11A1	2 Thermal Bands (31, 32) (10.780–12.270)	1 km (actual, 0.928 km)	Daily (daytime	Unit 16 (unsigned integer number)

When compared to geophysical methods, Thermal Infrared (TIR) remote sensing is a more cost-effective and time-efficient technique for detecting thermal anomalies in geothermal regions and
volcanoes. It also allows for large-scale operations. TIR data can be used to analyze geothermal anomalies in terms of land surface temperature (LST) and geothermal radiative heat flux (RHF). The heat flux from regions of geothermally heated earth has been directly measured using thermal imaging (Bromley *et al.*2011; Haselwimmer and Prakash, 2013; Wendy *et al.* 2014). The Landsat satellites are one of the spacecrafts that have been utilized to map thermal activity (Howari, 2015). Gemitzi et al. (2021) demonstrated the accuracy of identifying geothermal anomalies by remotely sensed land surface temperature (LST) of land covers and derived LST time series data from Landsat 8. Imagery from Landsat Thematic Mapper (TM) and Enhanced Thematic Mapper Plus (ETM+) has been used to map and evaluate volcanic features efficiently (Savage, 2009) A multitude of research investigations have utilized TM and ETM+ data to locate lineaments (such as fault lines) during the geothermal area exploration process (Bourgeois *et al*., 2000; Song *et al*., 2010; Qin *et al*.,2011). Qin *et al.*, (2011) used Landsat ETM+ thermal infrared data to explore geothermal areas in Teng Chong, China.

Ngene et al. (2022) carried out a Reconnaissance investigation of geothermal resources in parts of the Middle Benue Trough, Nigeria using remote sensing and geophysical methods. They used Landsat 8 scene to estimate the Land Surface Temperature in ArcGIS™. The LST results show lower temperature ($<30^0$ C) at the Awe and Wukari thermal springs than unknown rivers/streams discovered in Kwande (38^0 C), Ussa(38^0 C), Gwer East(37^0 C), Yola Cross, and Ogoja (36^0 C).

Idi et al. (2022) utilized Landsat 8 thermal infrared data to conduct spatial mapping and monitoring of thermal anomaly

and radiative heat flux in the vicinity of Lamurde hot spring, located in the upper part of the Benue trough in Nigeria. Their results revealed a significant seasonal variation in both outcrops, associated with elevated surface temperatures and heat loss anomalies throughout the year. The active geothermal area recorded peak LST values of 43.70 C, 35.60C, 29.40C, and 27.50C in January, April, July, and October, respectively. Recently Fagbohun et al (2024). Integrated magnetic and remote sensing methods for mapping geothermal signatures in the middle part of Benue Trough, Northeastern Nigeria. They used day-time Landsat 8 with ASTER daytime and night-time images for detailed geothermal anomaly mapping. Their results showed that Akiri, Awe, Azara, and Ribi display noticeable thermal anomalies in the night-time thermal anomaly map with Akiri thermal spring having the most prominent thermal anomalies. Although the remote sensing method is excellent for identifying geothermal resources, few geoscientists have applied this methodology within the Benue Trough, Nigeria, mostly focusing on Landsat 8 while neglecting other areas of the Trough due to its vastness. The research area, which includes the Middle and Upper Benue Trough of Northern Nigeria, is renowned for its abundance of warm/hot springs (Kurowska & Schoeneich2010). However, the precise locations and surface temperatures of these springs may not have been fully documented, either due to oversight or the emanation of new hot springs due to the subsurface geologic activities but with the improved satellite data (Landsat 9) resolution and processing technique, we intend to explore new possible geothermal zones. These warm springs provide information into the most likely geothermal sources. The geological structure, which may be detected by lineament analysis, is the primary factor controlling the spread of geothermal manifestations. The Fault and Fracture Density (FFD) approach is an easy approach for identifying lineaments (Suryantini and Wibowo, 2010). Dani *et al.,* (2020) stated that a region with a high density of faults and fractures is more likely to have geothermal manifestations distributed throughout it. Using technology for satellite imagery is one of the best ways to locate density lineaments and geothermal manifestation distribution. In this research, we aim to evaluate geothermal potential through remote sensing techniques in Northern Nigeria by analyzing lineament density and identifying high LST zones.

The region of coverage for the research is 166.5 km by 166.5km which is 27722.25 km^2 and composed of the following states: Plateau, Benue, Nassarawa, and Taraba. It is situated between longitudes of 8°30'0"E and 10°00'0"E; and latitudes of 8°00'0"N and 9°30'0"N. Geologically, the area of study covers Benue and part of Nassarawa is underlain by sedimentary basins while part of Nassarawa, Plateau, and Taraba is mainly of Basement Complex. The Precambrian gneiss, migmatites, and metasediments that underlie the Basement Complex in Nigeria's Northern region have been invaded by a sequence of granitic rocks from the late Precambrian to the Lower Palaeozoic (Annor, 1995; Obaje, 2009). Older Granite, a term for the plutonic rocks, was formed approximately 500–600 million years ago and represents the Pan-African orogeny in Nigeria. Mostly made up of granites, diorites, and dolerites, the older granites originate from Pan-African. (800–400 Ma, i.e. Neo-Proterozoic to Early Palaeozoic) The most prevalent form of rock in the Nigerian Basement complex is the migmatite-gneiss complex (Figure 1). Banded gneiss and biotite-gneiss comprised the majority of its composition. The biotitic gneisses, which are quite common, typically have significant foliation and fine grains due to the symmetrical arrangement of alternating dark and light minerals. The banded gneisses have complex band folding and alternate bands of light and dark color. The majority of the Basement complex is covered with belts of younger meta-sediments, which are significantly metamorphosed old pre-Cambrian sedimentary rocks that trend approximately north-south. The predominant geological formations in the region are the quartz-biotite-muscovite schist, which are relics of old shaly rocks. These metamorphose radially into micaceous schists with coarse grains that include feldspar. Commonly occurring schists include graphite, phyllites, and chlorite. Enormous spherical masses of older granite can be discovered within the older Migmatite gneiss complexes and schists are present across the Basement Complex. (Offodile,1976; Obaje, 2009) The ancient granites have a very different makeup. Younger granite complexes dominate the Jos Plateau in Nigeria, providing a unique assemblage of intrusive and volcanic rocks surrounded by ring faults or dykes.

Benue Trough is the Sedimentary Basin that underlies the study region. (Black & Girod, 1970) The Agwu-Ndeaboh Group, the Eze-Aku Group, the Nkporo Formation, and the Bima Formation are the Cretaceous sedimentary rocks that underlain the study region (Ahile *et al*,2024). In the western edge of the Abakaliki Anticlinorium, the Eze-Aku Group is conformally overlaid by the Awgu Formation but the Nkporo Group underlies it in the Afikpo Synclinoium, with the Awgu Formation abruptly missing. Awgu Shale is made up of well-bedded, dark, bluish-grey shales with a profusion of thin limestone and marl interbeds. The Afikpo Sub-basin's base lithostratigraphic unit, the Nkporo Formation (Campanian–Maastrichtian), is primarily composed of dark grey to black shales, sandstone, some limestone, and oolitic ironstone beds (Simpson, 1954)

In the Abakiliki Basin, a series of fossiliferous black shales and limestones make up the Awgu Formation. Shales, siltstone, sandstones, coals, and subsidiary limestone are interconnected in the Middle Benue Basin (Benkhelil, 1989). The oldest sedimentary unit in the Upper Benue Trough is the sandstone of the Bima formation. The bottom of the sedimentary sequence is made up of this Early Cretaceous Bima sandstone, which lies unevenly on the Pan African basement. The sandstone has uncommon sedimentary features and is not well stratified (Carter,1963). Finer materials are filled on its internal scouring surfaces. The sandstone beds lack significant lateral consistency and have inconsistent connections. Predominantly composed of mudstones, shales, and coarse- to medium-grained sandstones embedded in carbonaceous clays, this formation was formed during continental circumstances (fluvial, deltaic, lacustrine).

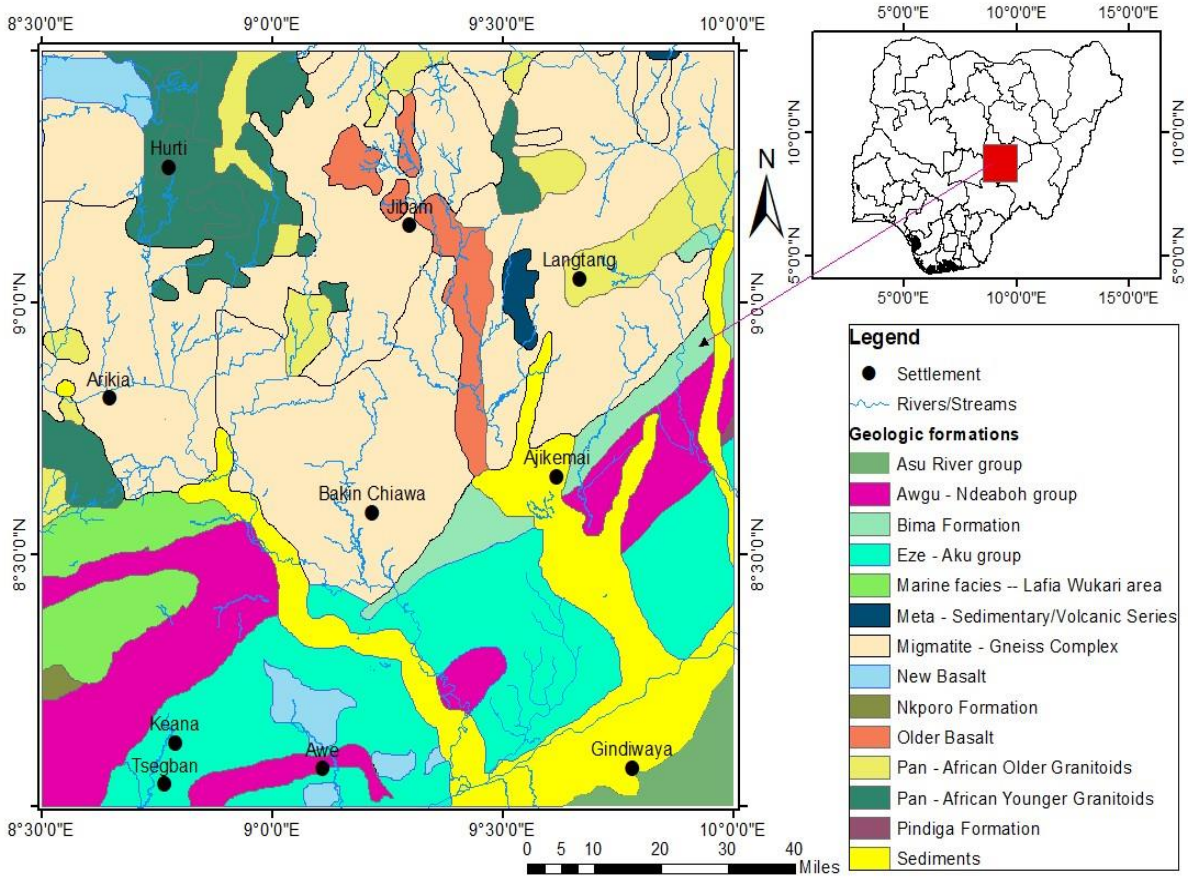

Figure 1: Geological background within the region (Ahile *et al*,2024)

MATERIALS AND METHODS

ArcMap10.7.1, *Google Earth Pro, and QGIS 3.36.3.* (Ngene, *et al*, 2022; Idi *et al*, 2022) and three Landsat 9 (OLI-2/TIR-2) scenes which were acquired on 2023-12-01, 2023-12-17, 2023-12-26 at "09:43:54.1646039Z", "09:44:19.6895310Z", "09:38:09.5605180Z" respectively and four digital elevation model (DEM) scenes with 1-ARC resolution acquired on 2000-02-11 00:00:00-06 and published on 2014-09-23 00:00:00-05 were retrieved at http://earthexplorer.usgs.gov/ on March 8, 2024. MOD11A1 V006 MODIS /Tera Land Surface Temperature/Emissivity Daily L3Global 1km SIN Grid 1 daytime data was obtained from http://Ipdaac.usgs.gov/ on 12th January 2025. Landsat images were chosen for their low cloud coverage (less than 10%). These imageries were meticulously chosen to encompass the middle and upper Benue trough of Nigeria which form the study area.

Satellite Data Processing Method

Measurement of land surface temperatures (LST)

The variables used to calculate Land Surface Temperature (LST) Landsat-9 include Top of Atmosphere (TOA) spectral radiance, TOA brightness temperature (BT), Normalized Difference Vegetation Index (NDVI), and Land Surface Emissivity (LSE).

Top of Atmosphere spectral radiance

Equation (1) demonstrates using the radiance rescaling factor, thermal infrared digital number, and spectral band to transform satellite imagery into TOA radiance.

$$L_\lambda = M_L * Q_{cal} + A_L \quad (1)$$

Where: L_λ =TOA spectral radiance (Wm^2 μm^{-1} sr^{-1} m^{-2}), M_L = Advanced multiplicative rescaling factor for band 10, A_L = Advance additive rescaling factor for band 10, Q_{cal} = Band 10, which were all obtained from the metadata.

Brightness temperature (TB)

Microwave radiation is measured as brightness temperature (BT) as it ascends from the uppermost layer of Earth's atmosphere. The constant thermal values are contained in the information that is appended to Landsat-9 data called metadata. Equation (2) was applied to these data to convert the BT's spectral brightness from Kelvin (K) to Celsius (^{0}C) degrees (Neinavaz, 2020).

$$BT = \frac{K_2}{In\left(\frac{K_1}{L_\lambda}+1\right)} - 273.15 \quad (2)$$

Where, ($K_1$and K_2 Constants for Band 10 Thermal Infrared Sensor in Landsat-9(Table 2), L_λ is the spectral radiance which was computed as shown in Equation 1

Normalized Difference Vegetation Index (NDVI)

NDVI is a measure of vegetation abundance that can also be used to assess vegetation health. It is related to biomass, chlorophyll content, and water stress. Vegetation health in geothermal locations is also influenced by changes in ground temperature and soil chemistry, particularly due to hydrothermal modification by acidic steam condensates. Vegetated areas have high near-infrared and low red visible reflectance (Mia *et al.*, 2012). NDVI which is computed using the near-infrared (band 5) and red (band 4) bands, shows the proportion of vegetation within a pixel or a region. The computation is done using the ratio of the Red and NIR band reflectance values. Sobrino *et al.* (2008), provided significant equations for calculating the emissivity from thermal infrared data using an NDVI-based approach that is also compatible with Landsat 8–9.

$$NDVI = \frac{NIR-RED}{NIR+RED} \quad (3)$$
$$NDVI = \frac{Band\ 5-Band\ 4}{Band\ 5+Band\ 4}$$

Where: Red = Red band values of band 4, NIR = Near-infrared band values of band 5

Land Surface Emissivity (LSE)

LSE is the mean emissivity of an element of the Earth's surface derived from estimated radiance and land surface temperature (Norman & Becker, 1995). LSE is a crucial component of predicting land surface temperature using Landsat 9 data. Measured radiance and LST compute the average emissivity of a surface element on Earth. Land Surface Emissivity must be calculated to be used in the estimation of LST. According to Ngene et al (2022), Equation 4 was used to first determine the total Proportion of Vegetation (Pv) before computing the LSE. The NDVI values from (Figure 1) which were obtained using Equation 3 were substituted into Equation 4 to compute Pv.

$$P_v = \left[\frac{(NDVI)-(NDVI)_{min}}{(NDVI)_{max}-(NDVI)_{min}}\right]^2 \quad (4)$$

Where:

NDVI represents digital values from an image, $(NDVI)_{min}$ represents the minimum digital values from the scene, and $(NDVI)_{max}$ represents the maximum digital values from the scene.

To estimate LSE, Sobrino *et al.* (2004) proposed Equation 5.

$$LSE = 0.004 \times P_v + 0.986 \quad (5)$$

Land Surface Temperature (LST)

Lastly, Equation (6) is adapted from (Weng et al, 2004) to compute the LST:

$$LST = \frac{BT}{\left(1+\left(\lambda \times \frac{BT}{c_2}\right) \times In(\mathbf{LSE})\right)} \quad (6)$$

Given that:

λ= Wavelength of emitted radiance(10.895)(Sobrino *et al*,2004), LSE =Land surface emissivity value, $c_2 = h \times \frac{C}{S} = 1.4388 \times 10^2 mK = 14388mK$, h = Planck's constant= $6.626 \times 10^{-34} Js$, S = Boltzmann constant $= 1.38 \times 10^{-23} Jk$, c = Speed of light $= 2.998 \times 10^8 m/s$.

Landsat and MODIS Imagery Processing

The study area coordinates were inserted into Google Earth Pro and the settlements within the area were extracted into kml format and were subsequently imported into QGIS 3.36.3 to create the shapefile of the settlements.

The Winrar 6.2.0.0 program was used to extract the Landsat-9 data one at a time. The files were then saved in folders labeled A1, A2, and A3, which corresponded to the data for each scene. There are 11 spectral bands (Bands 1 to 11) with unique band names in each of the obtained Landsat 9 imagery. Since bands 10, 5, and 4 will be used to calculate the LST in ArcMap10.7.1 using the raster calculator, they were chosen from A1, A2, and A3 and given new names to make them easier to identify. Each scene's chosen bands were loaded into ArcMap10.7.1 one at a time and made viewable side by side. Using the mosaic tool, all spectral bands were merged and given the names B_10, B_5, and B_4. Bands 5 and 4 of A1, A2, and A3 are contained in B_10, whereas band 10 of A1, A2, and A3 is contained in B_5 and B_4. Using the clip raster tool in ArcMap from B_10, the research region was cut. The LST (°C) was initially determined by using B_10 as an input raster for determining the TOA spectral radiance, and similarly, B_5 and B_4 to compute the NDVI, whose results were used to determine the BT and P_V, respectively.

Spectral radiance and Pv were also used to calculate the BT and the LSE. Subsequently, the LST was calculated using the BT and LSE output as input data. The Raster Calculator tool was used to complete the automated process. The land surface temperature variation in the Landsat is displayed in the layer of the computed LST. By using a chosen color ramp and symbology, regions with very high land surface temperatures are shown in red colour, moderate land surface temperatures in orange, and low land surface temperatures are displayed in green. The temperature range in the research area, from extremely low to high, is shown on the LST map (Figure 4). The LST was used to geo-reference the stream/river layers, which were then removed and created a new layer called "Stream/rives." The stream/river layers that symbolized the springs were taken into consideration during the meticulous selection of the high-temperate zones. The precise temperature readings and prospective geothermal potential locations were estimated using the identity tool. Five temperature classifications were produced using the Maximum Likelihood Classification tool (Figure. 4).

MOD11A1 V6.1 MODIS data was utilized to produce the MODIS_LST map in ArcGIS 10.7.1. These are ready-made data processed by the USGS using the split-window approach (Mao et al, 2005) and were transformed to LST after scaling with 0.02 (Zhengming, 2013). After the LST images were obtained from Landsat and MODIS, the statistical data of the images were evaluated, and the two data sets from Landsat and MODIS were classified using the Natural breaks method in the class of 10 break values each and correlated.

The veracity of LSTs derived from satellite data must be verified to provide dependable information regarding the quality of the LST for the aforementioned applications, as they contain a variety of corrections. Any data obtained from remotely sensed data cannot be used safely without validation, which is the act of independently evaluating the uncertainty of data from system outputs. The LST values obtained from the satellite data are verified using a variety of techniques; cross-validation, the temperature-based method (T-based), and the radiation-based method (R-based) are often employed techniques. (Li et al, 2013). In this study, we validated our result using the Pearson correlation.

Lineaments Density Extraction

The different Digital Elevation Model scenes (DEM) were loaded into ArcMap10.7.1 and were merged using the mosaic tool and a single scene was obtained where the raster was clipped within the study and was subsequently used to produce lineament using different Azimuth and altitude. The lineament density map (Figure 7) was subsequently produced from the lineament using ArcMap.

RESULTS AND DISCUSSION

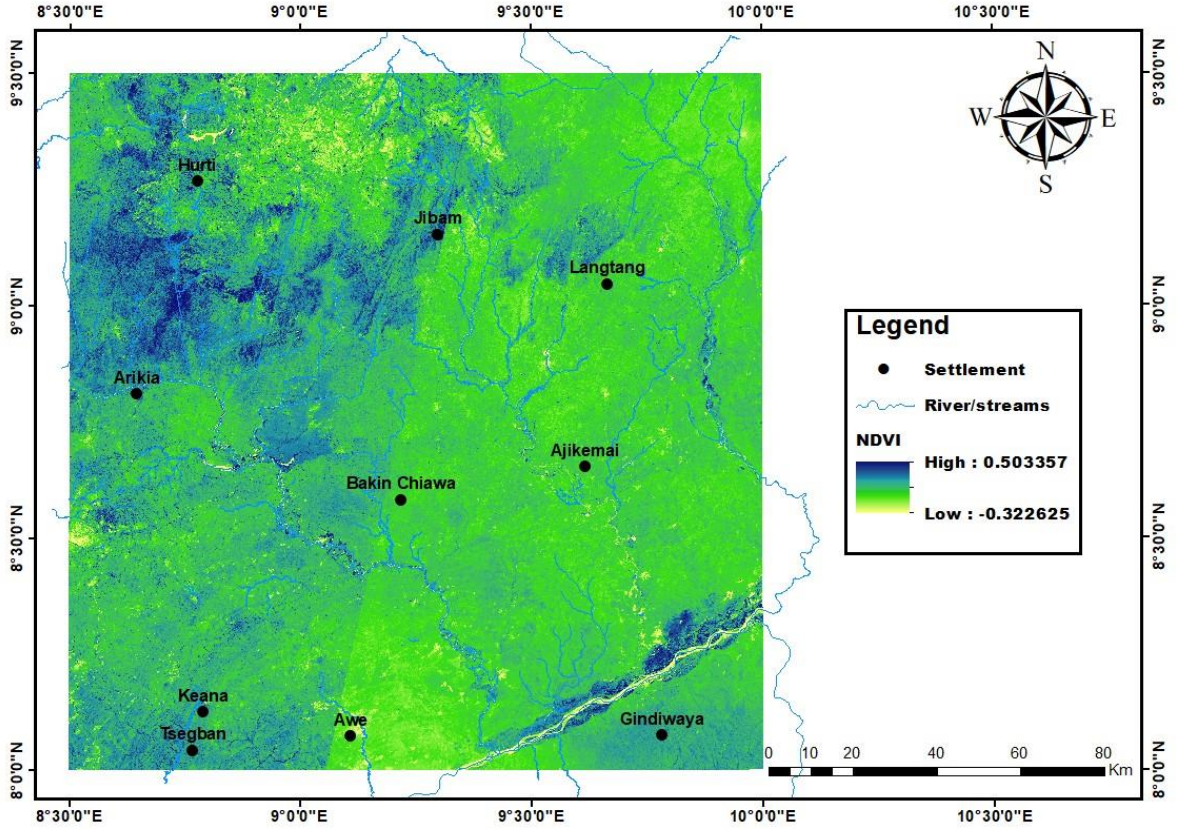

Figure 2: NDVI map

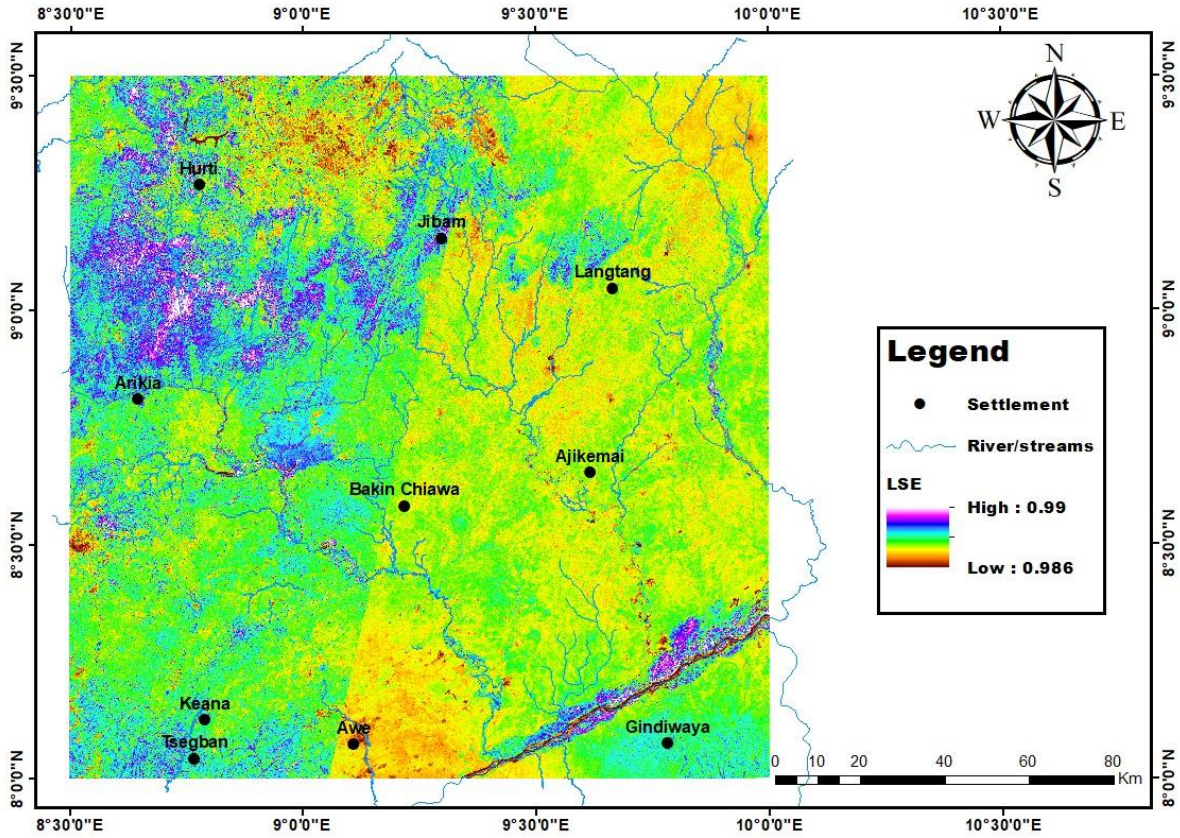

Figure 3: LSE map

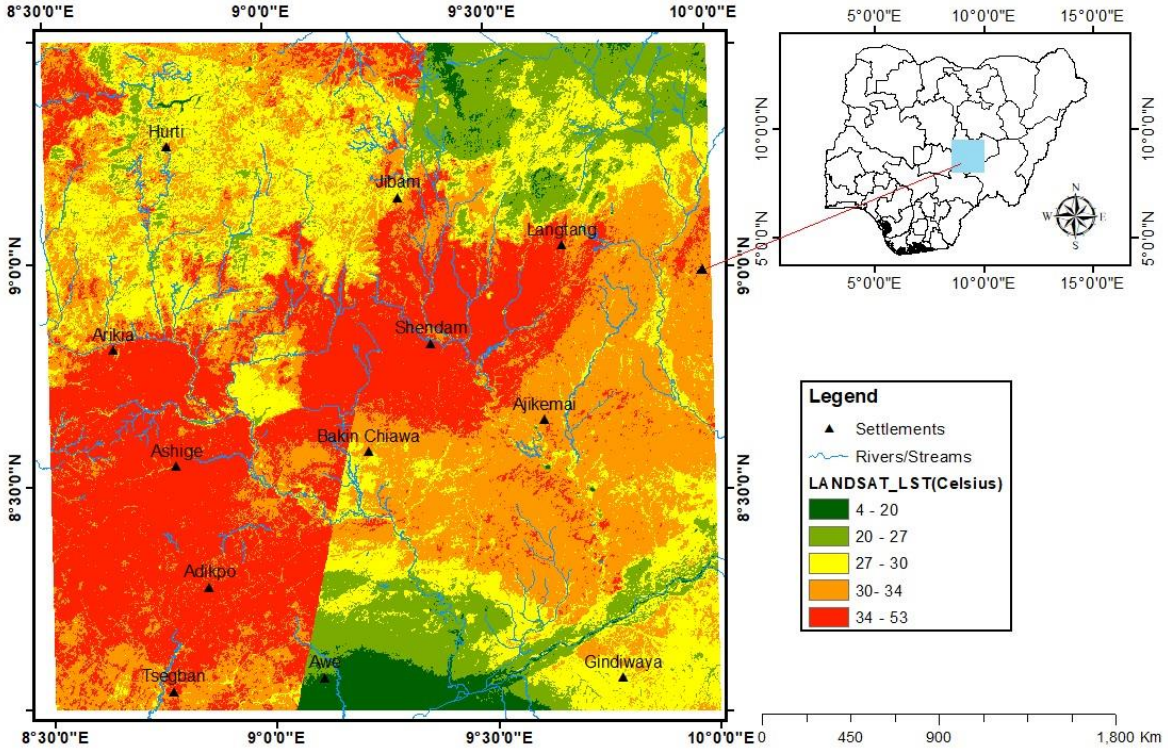

Figure 4: LST within the region using Landsat-9 thermal band

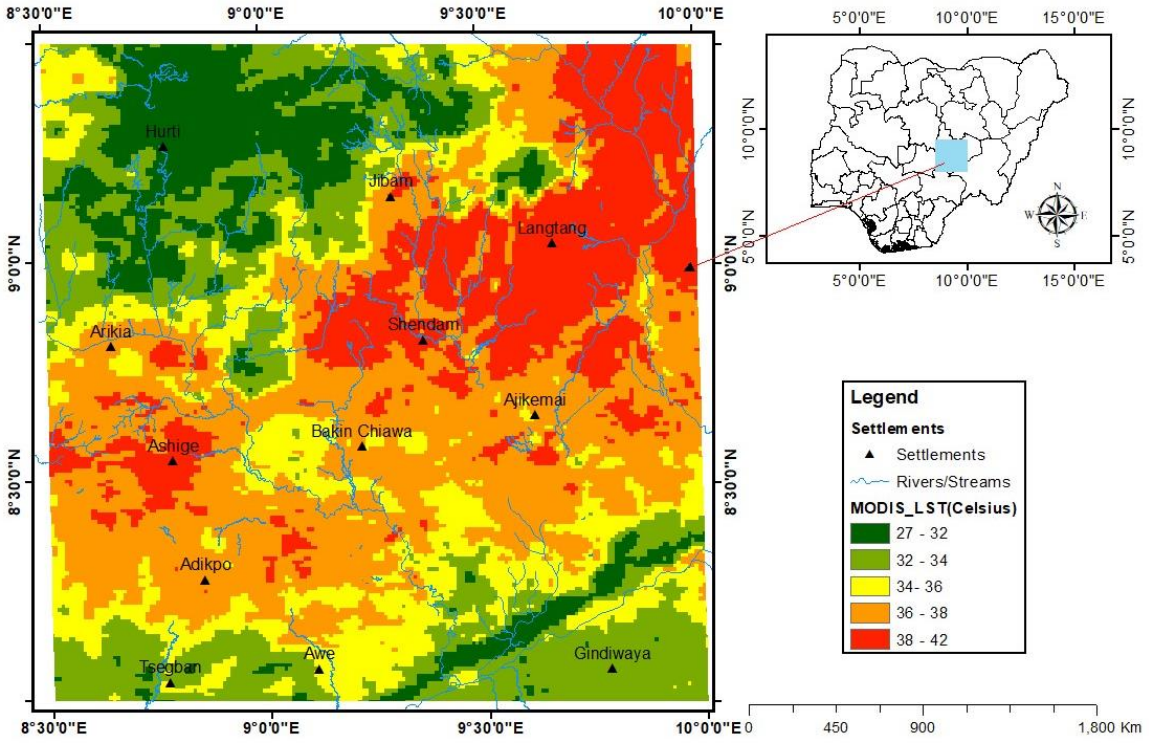

Figure 5: MODIS_LST map

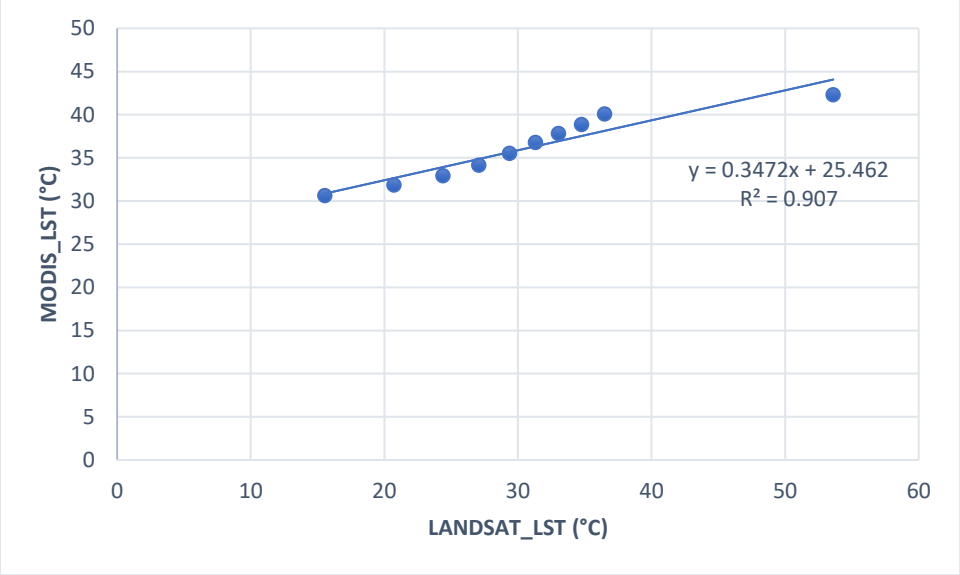

Figure 6: Correlation between Landsat_LST and MODIS_LST images break values

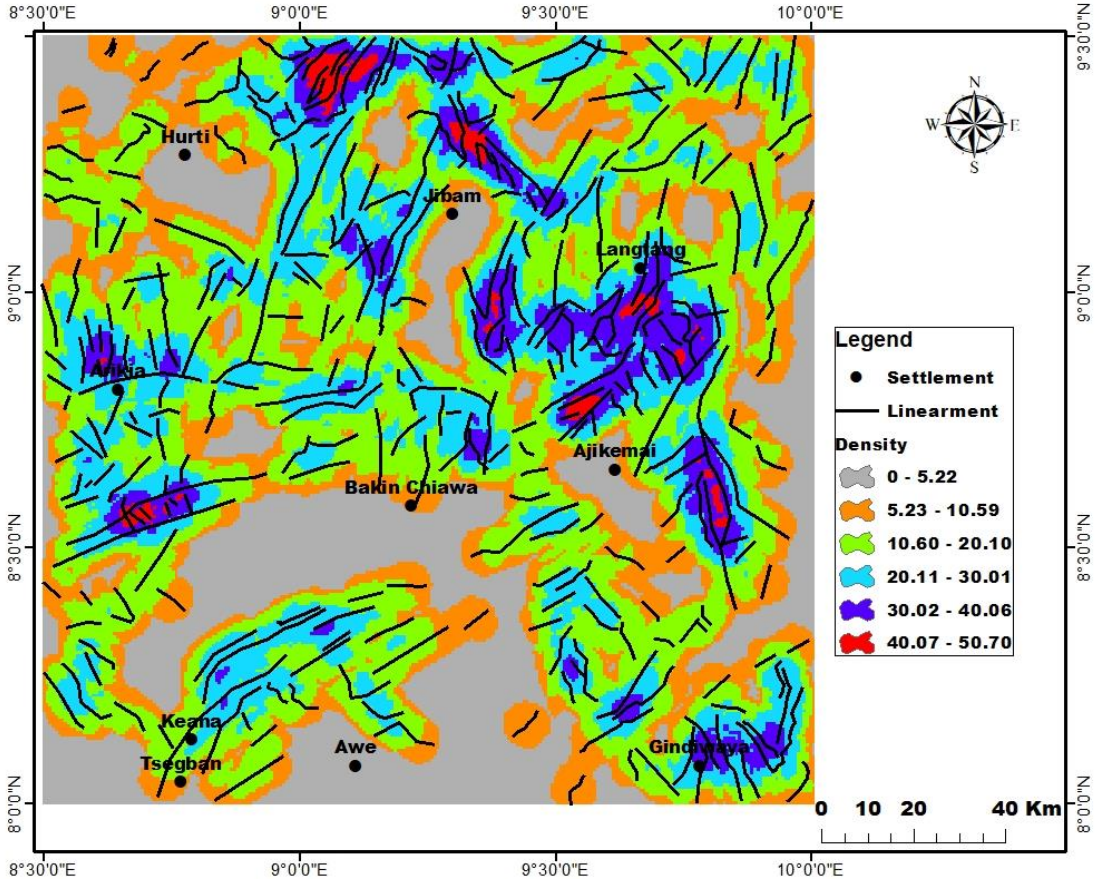

Figure 7: Lineament density within the region using DEM scenes

To validate LST results, the Pearson correlation coefficient was calculated between the Landsat_LST and MODIS_LST, results are highly correlated with each other (Figure 6) with the correlation coefficient of $R^2 = 0.907$. This result competes fairly with similar work of (Idi *et al*, 2022), within the Upper Benue Trough where the correlation was found to be ($R^2 = 0.801$). Elsewhere, Dervisoglu, (2013) did similar work in Istanbul, Landsat LST values, and MODIS data correlation was found to be ($R^2 = 0.88$). The observed variation between Landsat-9_LST and MODIS_LST values is due to the varied retrieval algorithms utilized in the computation, spatial resolution, spectral band, orbit and overpass time (Jiang & Lin, 2021).

The LST Maps (Figure 4 & Figure 5) show the range of land surface temperatures within the region, from relatively modest to high values. The high-temperate areas are considered the layers of streams/rivers that symbolize the springs. The thermal springs are probably found in or near the streams/rivers that reach the requisite high LST. There are no set standards for hot spring temperature because the

characteristics of warm springs vary depending on the geological setting of a region. Exploration geophysicists agree that the temperature of thermal or warm springs is higher at the discharge area than the yearly average air temperature (Ngene et al, 2022). The average mean surface air temperature in Nigeria is 27.3 °C, according to the World Bank Climate Change Knowledge Portal (2024), Common Hydrothermal low heat sources are just a little bit warmer than the surrounding air. Therefore, based on this assertion, we assume a warm/thermal spring/hotspot is 28 °C and above. The calculated LST shows some areas with temperatures above the average Mean Surface Air Temperature is 27.3 °C in Nigeria illustrating possible thermal springs.

When the lineament density (Figure 7) was compared with (Figure 1), those areas covered by Crystalline basement rocks, younger granites, and volcanic intrusive rocks around Langtang, Shendam, Jibam, Arikia, and Ashinge regions were observed to have high fracturing while the areas underlained by the Cretaceous sedimentary rocks around Awe, Keana, and Bakin Chiawa region shows relatively low lineament density. The high temperature was observed within those areas covered by basement complex, granites, volcanic intrusives; sandstones, and shales which agrees with the work of Ikumbur *et al.,* (2023). High geothermal heat flow and anomalously high lineament density are indicators of regions with considerable geothermal energy (Ike *et al.*2024; Kasidi and Nur 2013; Nuri, 2005). The complicated fault patterns and intersections point to an excessive density of lineaments around the hot/warm springs, when faulting occurs with basement rocks; the fracturing may improve permeability, facilitating the migration of geothermal fluids (Ngene, et al 2022). The lineaments around Aikri, Keana, Jibam, Langtang, and Ajikemi may provide proof of subsurface geological activities. Geothermal fluids may enter these faults and rise to the Earth's surface. The results obtained from Figure 4 and Figure 5 agree with the previous works of (Idi et al. 2022; Ngene et al, 2022; Fagbohun et al, 2024) who conducted similar research within the Benue trough and recorded LST values within the range. Therefore, it's intuitive sense that, as our study illustrates, locations with increased temperatures will be connected with geothermally active areas, such as warm springs. Possible warm or hot spring locations are found in the vicinity of Jibam, Langtang, Aikri, Ajikemi, Shemdam, and Ashige.

CONCLUSION

Geothermal potentials were evaluated through remote sensing techniques in Northern Nigeria. Throughout the study area, extremely low to very high LST values were found by geospatial analysis. The Pearson correlation coefficient was calculated between the Landsat_LST and MODIS_LST, results are highly correlated with each other with the correlation coefficient of $R^2 = 0.907$. A high density was found by lineament extraction in the Northern and southwestern sections of the studied region. Extremely high lineament density is correlated with high LST, primarily in the study area's basement complex. Fracture may increase permeability, enabling warm or hot springs to rise to the surface as geothermal fluids. The streams/rivers in or around the anticipated high LST are probably thermal springs, as they were overlaid on the LST, and high land surface temperature spots were identified. Areas with potential warm or hot springs include those at Jibam, Langtang, Aikri, Ajikemi, Shemdam, and Ashinge. The study thus proposes additional analysis of geothermal zones utilizing aeromagnetic and aero-radiometric data; an integrated strategy that can aid in the exploration of geothermal resource depth.

REFERENCES

Abraham, E. M., Obande, E. G., Chukwu, M., Chukwu, C. G. and Onwe, M. R. (2015). Estimating Depth to the Bottom of Magnetic Sources at Wikki Warm Spring Region, Northeastern Nigeria, Using Fractal Distribution of Sources Approach. Turkish Journal of Earth Sciences, 24(5), 494 512.

Ahile, J.A**.,** Meludu, O.C., Oniku, A.S, Sunu,S.A., Kenda, L.P., Kwarki, S. and Osumeje, J.O. (2024). Examination of the potential for geothermal energy in parts of the Benue trough, Nigeria, through the use of high-resolution aeromagnetic data. *Recent Advances in Natural Sciences*, 2 (2024) 124. https://doi.org/10.61298/rans.2024.124

Annual electricity production in Nigeria 2020-2021 report Published Doris Dokua Sasu, Nov 30, 2022 on https://www.statista.com/statistics/1294835/annual-electrical-energy-generation-in-nigeria/ downloaded on 2nd December,2022.

Annor, A. E. (1995). U-Pb Zircon age for Kabba-Okenegranodiorite Gneiss: Implication for Nigeria's Basement Chronology. African Geoscience Review, 2, 101 – 105.

Benkhelil, J. (1989). The origin and evolution of the Cretaceous Benue Trough, Nigeria. J Afr Earth Sci 8:251–282

Bourgeois, O., Dauteuil, O., and Van Vliet-Lanoe, B. (2000). "Geothermal Control on Flow Patterns in the Last Glacial Maximum Ice Sheet of Iceland," *Earth Surface Processes and Landforms*, 25(1):59–76

Black, R. and Girod, M. (1970). Late Paleozoic to recent igneous activities in West Africa and its relationship to basement structures. In: Clifford TW, Gass IG (eds) African magmatism and tectonics. Oliver and Boyd, Edinburgh, pp 185–210.

Bromley, C. J., Manen, S. M. van, and Mannington, W. (2011). Heat Flux from Steaming Ground: Reducing Uncertainties. In Proceedings, Thirty-Sixth Workshop on Geothermal Reservoir Engineering. Stanford, California.

Carter, J.D., Barber, W. and Tait, E.A. (1963). Geology of parts of Adamawa, Bauchi, and Bornu provinces in Northeastern Nigeria. Bull. Geol Surv. Nlgerta 30, 1- 108.

Dani, M., Agung, S. and Agung H. (2020). Revealing Geothermal Potential Areas with Remote Sensing Analysis for Surface Temperature and Lineament Density: Case Study in South Bajawa, NTT, Indonesia.*IOP Conference Series: Earth and Environmental Science*,417- 012009. https://doi.org/10.1088/1755-1315/417/1/012009 .

Dervisoglu, A. (2023). Investigation of the Efficiency of Satellite-Derived LST Data for Mapping the Meteorological Parameters in Istanbul. Atmosphere 14, 644. https://doi.org/10.3390/atmos14040644 .

on, R., Wenny, B. N., Poole, E., Eftekharzadeh Kay, S., Montanaro, M., Gerace, A., and Thome, K. J. (2024). Landsat 9 Thermal Infrared Sensor-2 (TIRS-2) Pre- and Post-Launch Spatial Response Performance. *Remote Sensing*, *16*(6), 1065. https://doi.org/10.3390/rs16061065 .

Fagbohun, B.J., Salawu, N.B. and Adepoju, S.A. (2024). Integrated magnetic and remote sensing methods for mapping geothermal signatures in the middle part of Benue Trough, Northeastern Nigeria. Remote sensing Applications: Society and Environment.37, https://doi.org/10.1016/j.rsase.2024.101434 .

Gemitzi, A., Dalampakis, P. and Falalakis, G. (2021). Detecting geothermal anomalies using Landsat 8 thermal infrared remotely sensed data. Int. J. Appl. Earth Obs. Geoinf. 96, 102283. https://doi.org/10.1016/J.JAG.2020.102283 .

Haselwimmer, C. and Prakash, A. (2013). Thermal infrared remote sensing of geothermal systems. Thermal Infrared Remote Sensing. 17. 453-473.

Howari, F.M. (2015). Prospecting for geothermal energy through satellite-based thermal data: Review and the way forward. Global J. Environ. Sci. Manage., 1(4): 265-274, https://doi.org/10.7508/gjesm .

Idi, B.Y., Maiba, A.I. and Abdullahi, M. (2022). The spatial mapping and monitoring thermal anomaly and radiative heat flux using Landsat 8 thermal infrared data-A case study of Lamurde hot spring, upper part of Benue trough, Nigeria. Journal of Applied Geophysics,203, https://doi.org/10.1016/j.jappgeo.2022.104654 .

Ike, E., Oniku, A.S., Ezike, S.C. and Wilson, R.E. (2024). Lithological and structural mapping of parts of southwestern Nigeria using aeromagnetic data. Recent Advances in Natural Sciences,2(54).

Jiang, Y. and Lin, W. (2021). A Comparative Analysis of Retrieval Algorithms of Land Surface Temperature from Landsat-8 Data: A Case Study of Shanghai, China. Int. J. Environ. Res. Public Health,18, 5659.

Kurowska E, and Schoeneich K (2010) Geothermal exploration in Nigeria. Proceedings of World Geothermal Congress, Bali, Indonesia, 25-29

Kasidi, S. and Nur A. (2013). Estimation of Curie Point Depth, Heat Flow, and Geothermal Gradient Inferred from Aeromagnetic Data over Jalingo and Environs North–Eastern Nigeria. International Journal of Earth Science and Engineering, 6(6), 294-301.

Kömürcü, M. İ. and Akpınar, A. (2009). Importance of geothermal energy and its environmental effects in Turkey. Renewable Energy, 34(6), 1611–1615. https://doi.org/10.1016/j.renene.2008.11.012 .

Li, Z.L., Tang, B.H., Wu, H., Ren, H., Yan, G., Wan, Z., Trigo, I.F. and Sobrino, J.A. (2013). Satellite-derived land surface temperature: Current status and perspectives. Remote Sens. Environ. 131, 14–37

Littleton, Colorado, Nov 30 (Reuters). In the article, Fossil fuels still dominate global power systems. https://www.reuters.com/markets/commodities/fossil-fuels-still-dominate-global-power-systems-2023-11-30/ assessed on 12th December,2024.

Maguire, G. (2023). Fossil fuels still dominate global power systems. Available on https://www.reuters.com/markets/commodities/fossil-fuels-still-dominate-global-power-systems-2023-11-30/ assessed on 3rd September 2024.

Mao, K., Qin, Z., Shi, J. and Gong, P. (2005). A practical split-window algorithm for retrieving land-surface temperature from MODIS data. Int. J. Remote Sens., 26, 3181–3204.

Mia, M. B., Bromley, C. J., and Fujimitsu, Y. (2012). Monitoring heat flux using Landsat TM/ETM+ thermal infrared data — A case study at Karapiti (‘Craters of the Moon’) thermal area, New Zealand. *Journal of Volcanology and Geothermal Research*, 235–236, 1–10. https://doi.org/10.1016/j.jvolgeores.2012.05.005 .

Neinavaz, E. Skidmore, A.K. and Darvishzadeh, R. (2020). Effects of prediction accuracy of the proportion of vegetation cover on land surface emissivity and temperature using the NDVI threshold method. Int J Appl Earth Obs Geoinformation, https://doi.org/10.1016/j.jag.2019.101984 .

Ngene, T., Mukhopadhya, M. and Ampana, S.(2022). Reconnaissance investigation of geothermal resources in parts of the Middle Benue Trough, Nigeria using remote sensing and geophysical Methods. Energy Geoscience, 3 (2022) 360-371, https://doi.org/10.1016/j.engeos.2022.06.002 .

Nuri, D.M., Timur U.Z., Mumtaz, H. and Naci, O. (2005). Curie Point Depth variations to infer the thermal structure of the crust at the African-Eurasian convergence zone, SW Turkey. *J. Earth planets Space*, 57, 373- 383.

Norman, J. M., and Becker, F., (1995). Terminology in thermal infrared remote sensing of natural surfaces. *Remote Sensing Reviews*, 12, 159–173.

Obaje, N.G. (2009). Geology and Mineral Resources of Nigeria, Lecture Notes in Earth Sciences, Springer, Berlin Heidelberg

Offodile, M.E., (1976). The geology of Middle Benue Trough, Nigeria, Special volume of Paleontological Institute, University of Uppsala, vol. 4, pp. 1-66.

Onyewuchi, R.A, Opara, A.I, Ahiarakwa, C.A and Oko, F.U. (2012). Geological Interpretations inferred from airborne magnetic and Landsat data: A case study of Nkalagu area, southeastern, Nigeria. *International journal of science and technology* 2 (4), 178-191.

Qin, Q., Zhang, N., Nan, P., and Chai, L. (2011). Geothermal area detection using Landsat ETM+ thermal infrared data and its mechanistic analysis—A case study in Tengchong, China. International Journal of Applied Earth Observation and Geoinformation. 13(4), 552-559.

Rajeshwari, A. and Mani, N.D. (2014). Estimation of Land Surface Temperature of Dindigul District Using Landsat 8 Data. *International Journal of Research in Engineering and Technology*,3(5),122-126.

Shahfahad, Talukdar, S., Naikoo, M.W.,Rahman, A.Gagnon, A.S.,Islam, A.T and Mosavi, A.(2023). Comparative evaluation of operational land imager sensor onboard Landsat 8 and Landsat 9 for land use land cover mapping over a heterogeneous landscape.38, (1), 2152496. https://doi.org/10.1080/10106049.2022.2152496

Sasu, D.D. (2023). Electricity generation in Nigeria in 2020 and 2021. https://www.statista.com/statistics/1294835/annual-electrical-energy-generation-in-nigeria/ accessed on 13th November 2024 at 5:20 pm.

Savage, S. (2009). Evaluating the Use of Landsat Imagery for Monitoring Geothermal Heat Flow in Yellowstone National Park. Land Resources and Environmental Sciences, Montana State University, Published CESU TASK AGREEMENT NUMBER: J1580050584.

Sekertekin, A. and Arslan,N. (2019). Monitoring thermal anomaly and radiative heat flux using thermal infrared satellite imagery – a case study at Tuzla geothermal region. *Elsevier*, http://www.elsevier.com/open-access/userlicense/1.0/ .

Simpson, A., (1954). The Nigerian Coal Field: The geology of parts of Onitsha, Owerri and Benue Provinces. Geological Survey Nigeria Bulletin., 24, 1- 67.
A, USA.

Sobrino, J. A., Jimenez-Munoz, J. C., Soria, G., Romaguera, M., Guanter, L., Moreno, J., and Martinez, P. (2008). Land Surface Emissivity Retrieval from different VNIR and TIR Sensors. IEEE Transactions on Geoscience and Remote Sensing, 46(2), 316–327. https://doi.org/10.1109/TGRS.2007.904834 .

Song, Y., Kim, H.-C., Yum, B.W., and Ahn, E. (2005) "Direct-Use Geothermal Development in Korea: Country Update 2000–2004," in Proceedings of the World Geothermal Congress, 1–7.

Suryantini and Wibowo H. H. (2010). Application of Fault and Fracture Density (FFD) method for geothermal exploration in the non-volcanic geothermal system: a case study in Sulawesi Indonesia Proceedings World Geothermal Congress 2010.

Wendy M. C., Elizabeth F. L. and Christopher, K. (2014). Remote Sensing of Geothermal-Related Minerals Resource Exploration in Nevada. Elsevier, (775) 784 – 1785

Weng, Q., Lu, D., and Schubring, J. (2004). Estimation of land surface temperature–vegetation abundance relationship for urban heat island studies. Remote Sensing of Environment, 89(4), 467– 483. https://doi.org/10.1016/j.rse.2003.11.005 .

Worldbank (2024). Observed Climatology of Average Mean Surface Air Temperature 1991-2020 in Nigeria. Available on https://climateknowledgeportal.worldbank.org/country/nigeria/climate-data-historical accessed on 25th June 2024.

Zhengming, W. (2013). Collection-6 MODIS Land Surface Temperature Products Users' Guide, ERI; University of California: Santa Barbara, CA, USA.